BRANCHING OF HERTZ CRACKS

H. P. Kirchner and R. M. Gruver[1]

INTRODUCTION

Impact by blunt, for example spherical, objects may cause Hertz cone crack formation in brittle materials (Figure 1). The cone cracks are similar in some respects to those formed by "static" indentations [1] but there are significant differences. For example, the relative absence of subcritical crack growth during impact leads to fractures at higher stresses and the expectation that crack branching will have a larger role in the fracture process. Crack branching of Hertz cracks in the impact surface is described in this paper. Branching of the main cone crack was reported previously [2].

PROCEDURES, RESULTS AND DISCUSSION

Soda-lime glass plates (6.35 mm thick and 79 mm diameter) were lightly abraded, stressed biaxially in flexure between concentric cylinders (diameters 15.3 mm and 33 mm) and impacted at various velocities on either the compressive or tensile surfaces by glass spheres (1.5 mm radius). The biaxial stresses were low relative to the impact stresses and were applied as part of a study of the effect of stress on penetration of surface damage and remaining strength which has been reported separately [2]. These stresses are not considered further in this paper. For most of the present specimens, conditions were chosen so that a minimum amount of surface damage was observed. This was done in order to have the simplest features available for characterization and analysis. Before impact, the impact surfaces were coated with a thin layer of soot. After impact the contact radius (r_{max}) was measured from the impression in the soot. Then, the soot was removed and the Hertz crack radius (r^*) was measured. The fracture surfaces were characterized by optical and scanning electron microscopy. Etching with hydrofluoric acid was used to bring out the fracture features.

Usually, Hertz cracks at surfaces have been described as a single circular crack or as concentric cracks. The crack patterns observed in the present investigation were much more complex and variable than would have been expected based upon these previous descriptions. The surfaces, prior to etching, show cracks with very ragged appearances. Etching reveals that the underlying cracks have much smoother contours (Figures 2 - 4). Apparently, at some stage during the impact cycle the forces transmitted across the cracks cause extensive formation of thin chips. Etching removes these chips revealing the underlying smooth curves.

The Hertz cracks may be partial cracks (Figure 2), completed cracks (Figure 3) or spirals (Figure 4). In Figure 2, the fracture origin is at the narrow portion of the crack pattern at the top of the photo. This fact

[1]Ceramic Finishing Company, State College, Pennsylvania, U.S.A.

has been confirmed. For example, hackle are observed in the surfaces of the cone cracks as shown in Figure 5. The fracture origins are located at the intersections of the hackle. Figure 2 also shows extensive crack branching. Figure 3 illustrates a just completed Hertz crack with the fracture origin at the top of the photo and extensive crack branching. In this case, r* measured horizontally across the surface is much greater than the height. This observation suggests that the portion of the crack shown in the top half of the photo formed during the first half of the impact cycle as the circle of maximum tensile (radial) stress expanded, and the lower half formed during the second half of the impact cycle as it contracted. In some cases, one side of the Hertz crack arrests while the other side continues to propagate. In these cases, spirals are formed as indicated in Figure 4. The outer portion of these spirals always appears to be a complex mass of cracks. Apparently, crack branching occurs during the first half of the cycle and continues during the contraction of the circle of maximum stress leading to the thick outer ring of cracks.

Confirmation of the normal sequence of fracture features is shown in Figure 6 which is a side view of the Hertz cone in which the fracture origin, mirror, mist and hackle are indicated.

For a particular material and set of test conditions, crack branching occurs at a constant value of stress intensity factor (K_B) as expressed by the following relation [3]

$$K_B = Y_B \sigma_f a_B^{1/2} \tag{1}$$

in which σ_f is the fracture stress, a_B is the crack radius at crack branching and Y_B is the geometrical factor appropriate for the crack at branching. In the present work, the mirror is considered to include the mist so that the fracture mirror radius and a_B are equivalent. K_B has been determined in tension and in flexure for numerous ceramics and glasses and several applications of this information have been demonstrated [3 - 7]. A strong correlation between K_B and Young's modulus (E) was observed [7] and used to suggest a strain intensity criterion for crack branching which permits prediction of K_B for various materials [8].

Hertz cracks originate at or very near the surface where the flaws are subjected to biaxial stresses. The radial stress (σ_{11}) is tensile and ideally at the contact radius has a magnitude of 0.261† times the average pressure (p_o) at the impact site. For ideal elastic impact the tangential stress is compressive at the surface. However, as shown by Evans et al [9], inelastic deformation at the impact site changes the tangential stress to tensile.

The radii at crack branching and equation (1) can be used to estimate the stresses at which the Hertz cracks form. To do this it is necessary to assume that the crack branching is adequately treated by considering only the principal tensile stress. Further, it is necessary to choose an appropriate geometrical factor Y_B. The portion of the Hertz crack nearest the surface extends about 50 μm into the specimen before flaring out to form the main cone. As long as the flaw size and the radius at crack branching are small relative to the depth of this portion of the crack and the contact diameter, it seems best to consider that the present case is approximated by a surface flaw loaded in tension, in which case Y_B

†Assuming Poisson's ratio of the glass is 0.239.

should be 1.12. However, near the surface the Hertz crack is not quite perpendicular to the surface. The effect of this inclination to the surface has not yet been investigated.

Two methods are available for measuring the crack radius at crack branching. One can locate the fracture origin in the impact surface as indicated in Figure 3 and measure the distance from the fracture origin to the first branch. Alternatively, one can project the hackle on both sides of the mirror to the surface as in Figure 6. Presumably, the fracture origin is located midway between the intersections of the hackle with the surface. A possible flaw, approximately at this location, is indicated in the figure. The radius at crack branching (a_B) is one half of the distance between the intersections of the hackle with the surface. There are numerous complications in making these measurements. A particular problem is that chipping frequently occurs near the fracture origin, obscuring needed features.

K_B has been determined for soda-lime and similar glasses in many experiments [3,5,10]. A representative value for soda-lime glass is 2.8 $MPa \cdot m^{1/2}$. Fracture stresses were estimated by substituting for a_B and K_B in equation (1) with the results shown in Table 1. The estimated stresses ranged from 228 to 559 MPa. Values of the ideal elastic stresses at the contact radius were calculated using [11]

$$\sigma_{11} = \frac{(1 - 2\nu)P}{2\pi r^2} \tag{2}$$

in which ν is Poisson's ratio and the load P is given by [12]

$$P = \frac{3E_1 r^3}{4CR} \tag{3}$$

in which E_1 is the Young's modulus of the glass plates (6.9×10^{10} Pa), C is a factor taking account of the elastic properties of the projectile and target with a value of 1.06. The calculations using equation (2) were based on the assumption that the fracture initiated when $r = r^*/1.2$. Therefore, these stresses were divided by 1.44 to estimate the magnitude of σ_{11} at r^*. This adjustment is based on the assumption that these stresses vary inversely as the square of the radius. These results are also included in Table 1.

The strengths of specimens that were not impacted were measured and averaged 91 MPa. Therefore, the fracture stresses at which the Hertz cracks form are several times the strength of the original material. These higher stresses reflect the fact that the stresses decrease rapidly with depth thus decreasing the stress intensity, the impacts do not usually occur near a severe flaw and there is less sub-critical crack growth under impact conditions.

The flaw sizes can be estimated using the method suggested by Krohn and Hasselman [13] who, assuming semi-circular surface flaws, calculated a mirror radius-flaw size ratio of 10. Flaw sizes calculated using this ratio are included in Table 1.

CONCLUSIONS

Detailed observations of Hertz cracks formed on surfaces by impacts of glass spheres on glass plates have shown that the shapes of the cracks are very complex and include partial, complete and spiral cracks. Crack branching is common and is clearly revealed by etching of the surfaces with hydrofluoric acid. The fracture stresses at which the Hertz cracks form were estimated from measurements of the radii at crack branching. To do this it was necessary to assume that the radial tensile stresses controlled the fracture process. The estimated fracture stresses ranged from 228-559 MPa, sometimes less than the calculated radial stresses but substantially greater than the measured strengths of the glass plates. Improvements in the method, especially to take account of the angle at which the crack is inclined to the surface, can be expected to yield improved results. The present results show that fractographic examinations of localized impact damage caused by blunt objects can aid in understanding the mechanisms by which the damage occurs.

ACKNOWLEDGEMENTS

This research was sponsored by the Office of Naval Research.

REFERENCES

1. LAWN, B. and WILSHAW, R., J. Mater. Sci. 10, 1975, 1049.
2. KIRCHNER, H. P. and GRUVER, R. M., Ceramic Finishing Company Tech. Rep. No. 4, Contract N00014-74-C-0241, 1976.
3. CONGLETON, J. and PETCH, N. J., Phil. Mag. 16, 1967, 749.
4. KIRCHNER, H. P. and GRUVER, R. M., Phil. Mag. 28, 1973, 1433.
5. MECHOLSKY, J. J., RICE, R. W. and FREIMAN, S. W., J. Amer. Ceram. Soc. 57, 1974, 440.
6. KIRCHNER, H. P., GRUVER, R. M. and SOTTER, W. A., J. Amer. Ceram. Soc. 58, 1975, 188.
7. KIRCHNER, H. P., GRUVER, R. M. and SOTTER, W. A., Phil. Mag. 33, 1976, 775.
8. KIRCHNER, H. P., To be published in the Proceedings of the Second International Conference on Mechanical Properties of Materials, Boston, (August, 1976).
9. EVANS, A. G., WILSHAW, T. R., CHESNUTT, J. C. and NADLER, H., Rockwell International Science Center First Report, Contract N00014-75-C-0669, 1976.
10. KIRCHNER, H. P. and SOTTER, W. A., Ceramic Finishing Company Technical Report No. 1, Contract N00014-74-C-0241, 1974.
11. LAWN, B. R. and WILSHAW, T. R., "Fracture of Brittle Solids", Cambridge University Press, New York, 1975, 20.
12. EVANS, A. G., J. Amer. Ceram. Soc. 56, 1973, 405.
13. KROHN, D. A. and HASSELMAN, D. P. H., J. Amer. Ceram. Soc. 54, 1971, 411.

Table 1 Estimated Fracture Stress and Flaw Size for Fracture Origins of Hertz Cracks

Spec. No.	Applied[1] Stress MPa	Impact Velocity ms^{-1}	Contact Radius r_{max} μm	Hertz Crack Radius (r*) μm	Crack Length at Branching (a_B) μm	Est. Fracture[2] Stress MPa	Calc. Fracture[3] Stress MPa	Est. Flaw Size μm
5	0	76	550	260	120[4]	228	406	12
6	43.1C	45	320	270	40[4]	395	422	4
11	57.5T	39	340(?)	350	20[5]	559	547	2
35	57.5C	55	420	380	60[4]	323	594	6

Note (1) T indicates tensile, biaxial flexural stress, C indicates compressive stress
(2) Crack branching method
(3) Ideal static stress assuming r = r*/1.2
(4) a_B measured on impact surface
(5) a_B measured on side of Hertz cone crack

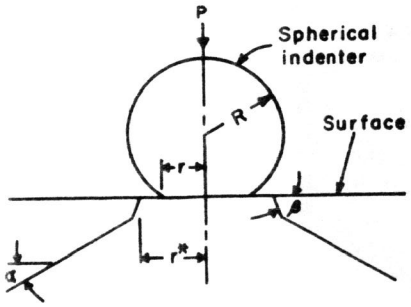

Figure 1 Hertz Crack

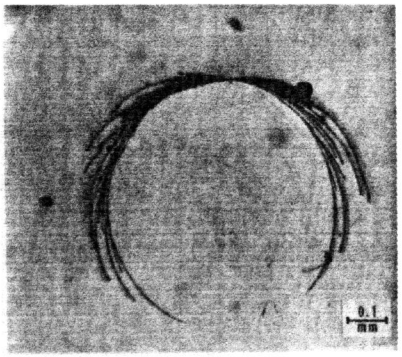

Figure 2 Partial Hertz Crack

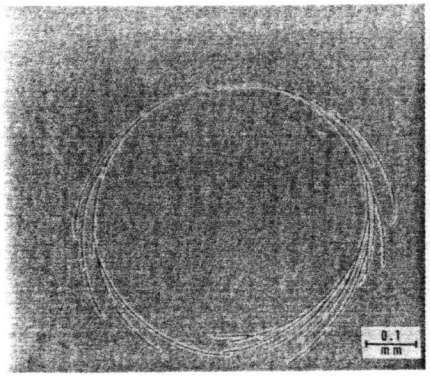

Figure 3 Complete Hertz Crack

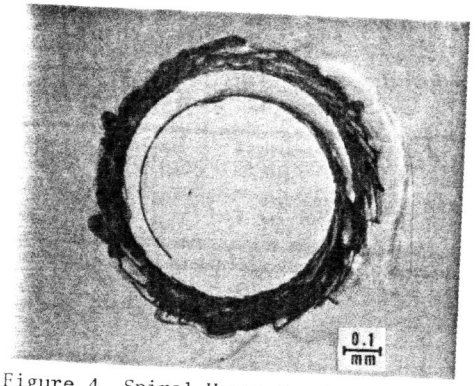

Figure 4 Spiral Hertz Crack

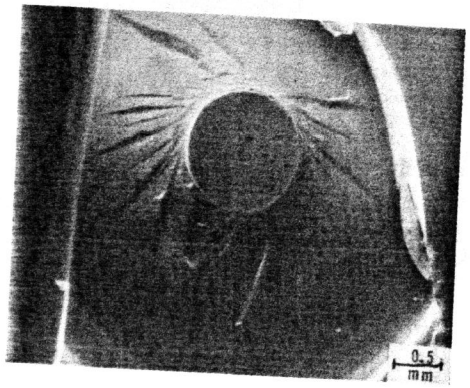

Figure 5 Hackle on the Surface of the Cone Crack

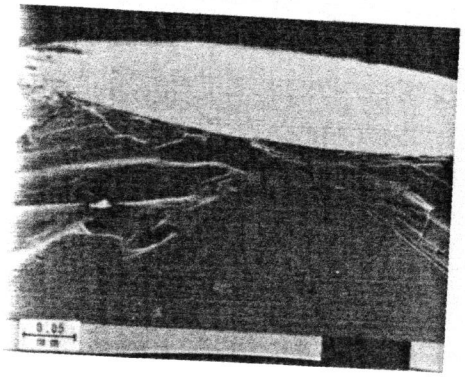

Figure 6 Side View of Hertz Cone